Laser Physics, Vol. 13, No. 4, 2003, pp. 644–651.

Carrier–Envelope Control of Femtosecond Lasers with Attosecond Timing Jitter

F. W. Helbing, G. Steinmeyer[1], and U. Keller

Ultrafast Laser Physics Laboratory, Institute of Quantum Electronics, Swiss Federal Institute of Technology, ETH Hönggerberg-HPT, CH-8093 Zürich, Switzerland

e-mail: steinmey@mbi-berlin.de

Received September 9, 2002

Abstract—In the generation and applications of few-cycle laser pulses, the relative phase between the carrier and envelope plays an important role. In laser oscillators, fluctuations of the carrier–envelope phase are found to be highly irregular. Several mechanisms contributing to the carrier–envelope-phase noise are identified. We analyze thermal contributions, amplitude-to-phase conversion mechanisms, and beam-pointing induced effects. Based on our analysis, we can avoid or reduce certain mechanisms. This is demonstrated with a highly stabilized oscillator which displays a residual carrier-envelope-phase noise of a few mrad over integration times of a minute. The residual noise of the stabilized laser corresponds to a timing jitter between the carrier and envelope of 10 attoseconds. Control of the carrier–envelope phase to this degree is an important prerequisite for the exploration of phase-dependent nonlinear optical effects and may also be useful in frequency metrology.

1. INTRODUCTION

Recent advances in ultrashort pulse generation have pushed pulse durations down to a few femtoseconds [1]. Some of the shortest pulses generated to date have a width equivalent to about two optical cycles [2–6]. When pulse durations approach this regime, the commonly used approach of the slowly varying envelope approximation (SVEA) starts to fail. Nonlinear optical effects, such as second-harmonic generation, are then expected to depend not only on the envelope structure of the pulses but also on the structure of the electric field itself, including its relative phase to the envelope, which has been referred to as the absolute phase. Recently, some first experimental evidence for the failure of the SVEA was reported [7]. In that study, the energy distribution of electrons generated by multiphoton ionization (MPI) was investigated. An anticorrelation of the electron energies was detected between MPI electrons ejected in opposite directions. This effect was only observed for the very shortest 6-fs pulses available in that study, but not for longer pulses. However, a direct correlation with measurements of the relative phase between the carrier and envelope has not been experimentally confirmed yet.

Given the electric-field structure of an optical pulse $E(t)$, the conversion efficiency $\eta^{(n)}$ for a nonlinear process of order n can be estimated from

$$\eta^{(n)} \propto \int E(t)^{2n} dt. \quad (1)$$

For a simple estimation of the severity of phase effects of few-cycle pulses, we separate the carrier and envelope, assuming that

$$E(t) = A(t)\cos(\omega t + \varphi_0). \quad (2)$$

The envelope function $A(t)$ has to be carefully chosen to ensure energy conservation, i.e., $\eta^{(1)} \equiv \text{const}$, and a vanishing DC part ($\int E(t)dt \equiv 0$) when varying the absolute phase [8] of the pulse. For the computations in Fig. 1, we have chosen

$$A(t) = A_0 + A_1 \operatorname{sech}(t/t_0), \quad (3)$$

where A_0 and A_1 have been chosen to fulfill the above-mentioned criteria. To evaluate the carrier–envelope-phase sensitivity of $\eta^{(n)}$, we calculate the quantity

$$\Delta^{(n)} = \frac{\eta^{(n)}(\varphi_0 = 0)}{\eta^{(n)}(\varphi_0 = \pi/2)} - 1. \quad (4)$$

Figure 1 depicts the behavior of $\Delta^{(n)}$ for pulses of one to eight cycles in duration and nonlinear optical effects up to order $n = 50$. For pulse durations of more than three cycles and $n \le 6$, it appears virtually impossible to measure any deviation of the quantity from zero. With current technology and pulses of two or more cycles in duration, one has to employ highly nonlinear processes for a measurable effect. In this regime, the strongest effects are expected for high-harmonic generation processes, where n can be on the order of 100 or greater. For low-order processes, such as second-harmonic generation or two-photon absorption, a noticeable phase-dependence is only expected for pulses approximately one cycle or less in duration. These considerations make it clear that, with current ultrafast technology, direct observation of the break-

[1]Author to whom correspondence should be addressed:
Present address: Max-Born-Institut für Nichtlineare Optik und Kurzzeitspektroskopie, D-12489 Berlin, Germany.

down of the SVEA is more likely to be detected with amplified short pulses than at the oscillator level, where sub-two-cycle pulses are required for a measurable effect. In this paper, we will first describe methods to monitor changes of the absolute phase. We will then discuss jitter measurements of the phase between the pulse carrier and envelope in a femtosecond laser. We will trace back the origin of this noise. Based on the understanding of the underlying noise mechanisms, we describe the setup of a femtosecond oscillator with a rigorously controlled drift of the absolute phase.

2. BASIC DEFINITIONS

The relative phase between the carrier and envelope of an ultrashort pulse (the carrier-envelope-offset phase or CEO phase [9]) changes on propagation through a dispersive medium. The envelope travels at group velocity $v_g = c/n_g = c/(n + \omega dn/d\omega)$, whereas the underlying electric field structure, i.e., the carrier, propagates at phase velocity $v_\varphi = c/n$. This means that a pulse will undergo a permanent change of the CEO phase in a dispersive medium. When propagating through a dispersive material with an index of refraction $n(z)$ along an axis z, the pulse will accumulate a CEO phase change of

$$\Delta\varphi_{\mathrm{CEO}} = \left[\frac{2\pi}{\lambda}\int_0^L n_g(z) - n(z)dz\right]\mathrm{mod}\,2\pi = \left[\frac{\omega}{c}^2\int_0^L \frac{dn(z)}{d\omega}dz\right]\mathrm{mod}\,2\pi, \quad (5)$$

where L is the length of the dispersive material. Note that it is the first-order dispersion term $dn(z)/d\omega$ which gives rise to differing group and phase velocities in a medium. A case of particular importance is propagation through a laser cavity, as used in the generation of ultrashort pulses. In such a cavity, the pulse accumulates the CEO phase change of Eq. (5) every round trip and L takes the role of twice the cavity length. For a typical Ti : sapphire laser cavity, such as that described in [6], the roundtrip phase shift between the carrier and envelope from the 2.3-mm Ti : sapphire crystal, a 3-m air path, and the prism compressor can be estimated as about 250 optical cycles. However, only the fractional part of this phase shift is included in the $\Delta\varphi_{\mathrm{CEO}}$. As long as the cavity dispersion does not vary, the CEO phase will evolve strictly linearly with a constant phase change $\Delta\varphi_{\mathrm{CEO}}$ per round trip time $T_R = 1/f_{\mathrm{rep}}$. For the following, it is useful to define the CEO frequency [9]:

$$f_{\mathrm{CEO}} = \frac{\Delta\varphi_{\mathrm{CEO}}}{2\pi} f_{\mathrm{rep}}. \quad (6)$$

In the case of constant intracavity dispersion, this CEO frequency is constant. Note that even the tiniest changes of intracavity dispersion will give rise to a measurable change of the CEO frequency. In the case of the above-mentioned Ti : sapphire laser, e.g., a 10^{-6} change of cavity dispersion will already cause a 25-kHz shift of the CEO frequency. This consideration immediately demonstrates the necessity to shield the laser cavity from environmental influences when excessive fluctuations of the CEO frequency need to be avoided.

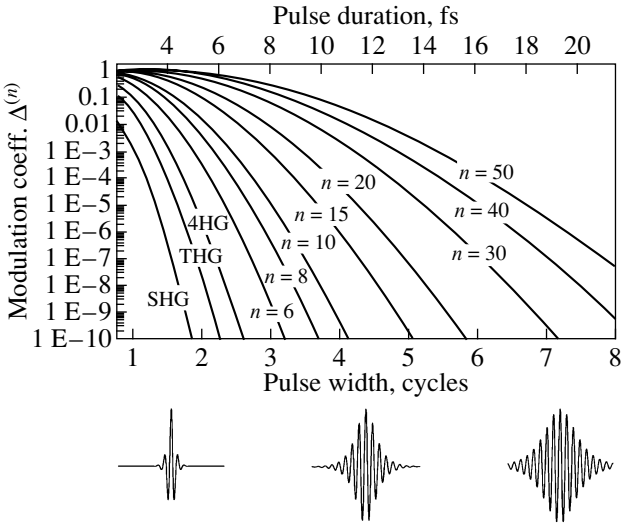

Fig. 1. Sensitivity to carrier–envelope effects $\Delta^{(n)}$ as a function of pulse duration for nonlinear processes of different order n. Orders $n = 2$, 3, and 4 are designated by SHG, THG, and 4HG, respectively. The bottom axis refers to the FWHM duration of the intensity envelope of the pulse in optical cycles, i.e., in units λ/c. The top axis designates pulse duration in femtoseconds for a center wavelength of the pulse of 800 nm (Ti : sapphire wavelength range). The time axes of the electric field representations in the bottom part of the graph are centered at the respective pulse width on the pulse width axis of the plot.

3. MEASUREMENT OF THE CEO PHASE

The electric field structure of an optical pulse cannot be directly accessed by any measurement. In the following, we will describe how the CEO phase can be accessed by an indirect measurement employing heterodyning of two different harmonics of the laser field. We will also show how the CEO and absolute phase are related to each other.

The field of a short laser pulse can be written as

$$E(t) = A(t)\exp(i\omega_c t + i\varphi_0), \quad (7)$$

where ω_c is the (angular) carrier frequency, $A(t)$ is the envelope function, and φ_0 is the absolute phase of the pulse. In the spectral domain, we can rewrite Eq. (7) as

$$\tilde{E}(\omega) = \tilde{A}(\omega)\exp(i\varphi_0). \quad (8)$$

The field of the second-harmonic of $\tilde{E}(\omega)$ is then written as

$$\tilde{E}^{(\mathrm{SH})}(\omega) = \gamma\int_0^\infty \tilde{E}(\omega')\tilde{E}(\omega-\omega')d\omega' = \gamma\exp(2i\varphi_0)\int_0^\infty \tilde{A}(\omega')\tilde{A}(\omega-\omega')d\omega', \quad (9)$$

where the proportionality factor γ includes the second-order susceptibility and a constant phase shift. Note that the second-harmonic field $\tilde{E}^{(\mathrm{SH})}$ is centered at $2\omega_c$ while the fundamental field $\tilde{E}$ reaches its maximum at ω_c. The main consequence of Eq. (9) is that absolute phases add up in sum-frequency generation processes. In the same way, absolute phases will subtract in difference-frequency generation processes. This is well known for optical rectification in the generation of THz waves [10] and can also be employed to generate mid-IR waveforms with a static absolute phase. Parametric amplification may also be used to generate pulses with static φ_0 [11].

Let us consider a delayed superposition of both fields $\tilde{E}^{(\mathrm{SH})}$ and $\tilde{E}$ at a frequency ω in the area of spectral overlap of the fundamental and second harmonic:

$$\begin{aligned}\tilde{I}(\omega) &\propto \left|\tilde{E}^{(\mathrm{SH})}(\omega) + \tilde{E}(\omega)\right|^2 \\ &= \left|\exp(i\varphi_0)\tilde{A}(\omega) + \gamma\exp(i\omega\Delta t + 2i\varphi_0)\tilde{A}^{(\mathrm{SH})}(\omega)\right|^2 \\ &= \left|\tilde{A}(\omega)\right|^2 + \gamma^2\left|\tilde{A}^{(\mathrm{SH})}(\omega)\right|^2 + 2\gamma\left|\tilde{A}(\omega)\tilde{A}^{(\mathrm{SH})}(\omega)\right| \\ &\quad\times\cos(\omega\Delta t + \varphi_0 + \pi/2).\end{aligned} \quad (10)$$

In the following, we will only consider the cosine term, which gives rise to a spectral interference signal if the delay Δt is chosen a nonzero value. Detection of this interference signal allows the determination of the absolute phase φ_0 in principle. Dispersive effects, however, will typically prevent a direct determination of the absolute phase using spectral interferometry. Still, this method allows the monitoring of shot-to-shot changes of φ_0, as has been described in [12–14]. This method requires acquisition of a complete spectrum per individual laser shot. Therefore, spectral interferometry cannot be directly used with MHz repetition rates of oscillators. In the latter case, let us reconsider Eq. (10) with $\Delta t = 0$ and a varying absolute phase $\varphi_0(t)$. In the case of a linear phase evolution $\varphi_0(t) = 2\pi f_0$, the interference term in (10) gives rise to a beat signal with constant frequency f_0. This beat signal is exactly synchronous with relative phase changes between the carrier and envelope of the pulse propagating through the laser cavity. One can therefore identify the frequency of the beat note as $f_0 = f_{\mathrm{CEO}}$. The connection to the previously defined CEO phase is then given by

$$\Delta\varphi_{\mathrm{CEO}} = \frac{1}{f_{\mathrm{rep}}}\frac{d\varphi_0(t)}{dt}, \quad (11)$$

which also holds in the more general case of varying intracavity dispersion. Note that neither the spectral interferometry method for single shot CEO phase measurement [12] nor the narrowband heterodyning schemes [9] used with mode-locked oscillators allows determination of the absolute phase. In fact, all methods monitor changes in the absolute phase with time, which is effectively proportional to the CEO phase according to Eq. (11).

4. MEASURING AND STABILIZING THE CEO FREQUENCY OF A FEMTOSECOND LASER

For experimental realization of the heterodyne detection scheme, we additionally broaden the laser output spectrum through white-light continuum generation in a microstructure fiber [15], regardless of the laser used. To some extent this may be disputable, because pulse fluctuations may also give rise to changes in the CEO phase via an amplitude-to-phase coupling mechanism inside the fiber [16]. This may appear particularly cumbersome because of the much higher nonlinearity of the microstructure fiber. However, as the fiber is placed outside the laser cavity, nonlinear or thermally induced phase changes will not add up as they do for intracavity, as will be shown in more detail below. This means that a change of first-order dispersion in the laser gain crystal affects the CEO frequency, whereas a change of dispersion in the fiber affects only the CEO phase in a single pass. For measuring the CEO frequency, we heterodyne the fundamental and the second harmonic of the microstructure fiber continuum [17]. For frequency-doubling of the long-wavelength components at 1060 nm, an LBO crystal is used to generate the second harmonic with noncritical phase matching. Given the 1-cm crystal length, one calculates a phase-matching bandwidth of about 4 nm. Note that all modes within the phase-matching bandwidth contribute to the beat signal. Fundamental and SHG components at 530 nm are heterodyned in a Michelson interferometer. Careful optimization of the arm lengths in this interferometer is required for detection of the beat signal. Experimental parameters of the laser were set to ensure maximum intensity and stability of the continuum components at 1060 and at 530 nm.

Figure 2 shows the setup employed and a typical rf spectrum measured by this setup. The CEO beat note and its mirror frequency are clearly visible at 35 and 65 MHz. The measured signal level is 45 dBc in a 300 kHz bandwidth. In our experiments, we found a signal level of at least 30 dBc necessary for reliable locking of the carrier-envelope-offset frequency. In the unstabilized laser with prism dispersion compensation, the frequency of this beat note may change very rapidly by up to several MHz in one second. This behavior is most likely due to air turbulence and is already strongly reduced by enclosing the laser in a box. Excursions of

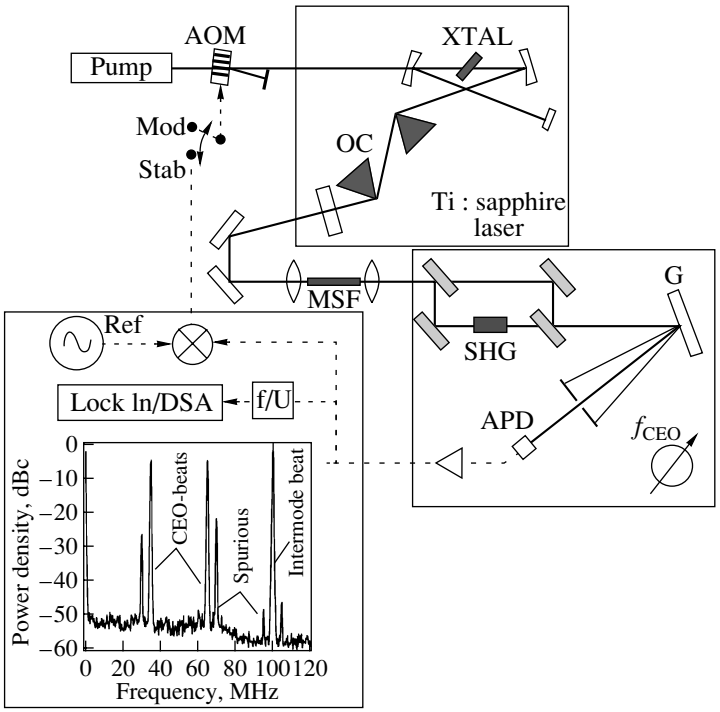

Fig. 2. Measurement and stabilization setup employed in the experiments. AOM: acoustooptic amplitude modulator. Note that the modulator is operated near 100% transmission and only a small portion of the pump beam is deflected onto a beam dump. XTAL: Ti:sapphire laser crystal. OC: output coupling mirror. MSF: microstructure fiber, used for spectral broadening beyond one optical octave. SHG: 1-cm long LBO frequency-doubling crystal, noncritically phase-matched for the generation of 530-nm light at 155°C. G: grating. APD: silicon avalanche photodiode. Ref: Synthesized rf reference oscillator, HP8663A. *f*/*U*: frequency-to-voltage generator, used to measure frequency noise densities as described below. The bottom left insert depicts an rf spectrum of the signal recorded by the APD detector. The signal consists of an intermode beat at 100 MHz, the CEO beat note and its mirror frequency, and several spurious component been generated by nonlinearities in the electronics.

the CEO frequency are further decreased by switching over to a prismless laser setup. With these improvements and still without any active stabilization, the CEO frequency stays within a 500-kHz interval for observation times of several minutes. Given the high sensitivity of the CEO frequency towards environmental changes, alignment of the cavity, etc., the CEO frequency of a femtosecond oscillator can be controlled in many different ways. Tilting of the end mirror in the prism arm of the laser was described as one of the first methods to adjust the CEO frequency [18]. While this has the advantage of orthogonalizing control of the cavity group and phase delay, this control is typically limited by the inertia of the mirror to below 1 kHz. Also, it cannot be used in prismless cavities. We control the CEO frequency by changing the laser pump power instead [19]. Figure 3 shows a transfer function, i.e. the measured change of CEO frequency induced by an acoustooptic amplitude modulator, which is located between the pump laser and Ti : sapphire laser. The physical mechanism behind this means of control is a change of the refractive index of the Ti : sapphire gain crystal, which can either be induced by temperature changes or self-refraction. To alleviate a comparison with theoretical estimates in Section 6, we plot the transfer function in units of the frequency change over the change in the intracavity peak intensity (Hz m^2/W). Clearly, a transition from a thermally dominated regime at low modulation frequencies to a self-refraction regime at kHz modulation frequencies can be seen. In the latter case, the transfer coefficient levels out at about 10^{-8} Hz m^2/W, whereas thermal contributions can give rise to about five-times stronger amplitude-to-phase coupling in the oscillator.

The combination of the measurement scheme and the control via modulation of the pump power is used to establish a phase lock of the CEO frequency to an external reference oscillator. The schematic setup of the servo loop is depicted in Fig. 4. The measured CEO beat signal is isolated and amplified and then mixed with a reference oscillator using a double-balanced mixer (MiniCircuits ZP3). The intermediate frequency signal is then fed into the input of the pump power modulator. The overall loop gain is adjusted for a sufficient phase margin to suppress parasitic oscillation of the servo loop. For stabilized operation, the laser pump power is adjusted within less than 1% of the maximum power. This range is typically found sufficient with the high passive stability of the prismless oscillator and allows for minutes of stabilized operation. A coarse adjustment of the CEO frequency can be achieved by slightly tilting a thin Brewster-angled intracavity glass

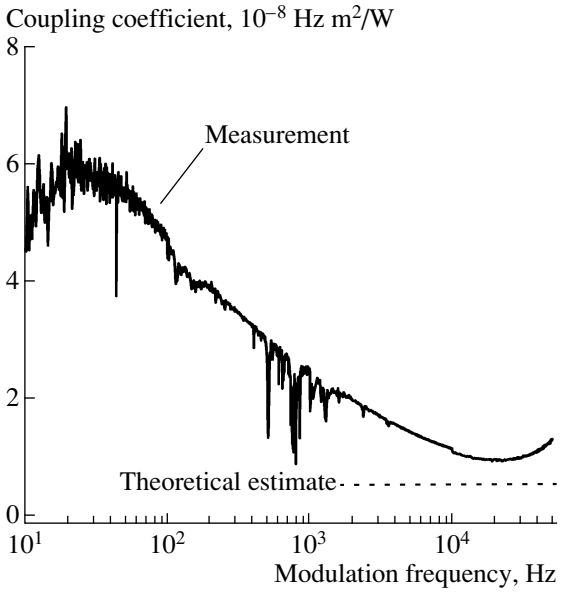

Fig. 3. Transfer function df_{CEO}/dI measured as a function of modulation frequency. The modulation of the intracavity peak intensity at the location of the Ti:sapphire gain crystal (XTAL) was achieved by modulating the pump power with the AOM shown in Fig. 2. The modulation index was kept at a perturbational level. This ensures stable operating parameters of the laser but does not fully suppress interference by laser noise at some isolated frequencies. For comparison, the theoretical estimate derived from the dispersion of the Kerr effect is also shown as a dashed line. Higher experimental values at low frequencies are explained by thermal contributions to the transfer function.

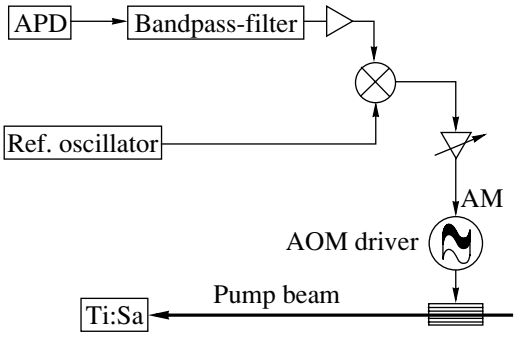

Fig. 4. Schematic setup of the stabilization experiments. One of the beat signals shown in the inset to Fig. 2 is isolated by a bandpass filter. The signal is mixed with the reference oscillator and fed back to the pump power modulation. The servo loop gain is adjusted to provide a sufficient phase margin for stable operation of the loop.

plate, which is also used for fine tuning of intracavity dispersion. One limitation of the current loop design is the acoustic delay between the actuator and optical beam inside the modulator. Still, we reach a servo loop bandwidth of 30 kHz, which is superior to any mechanical adjustment of the CEO frequency. The performance of the servo loop in terms of residual phase noise will be characterized in the following section.

5. CEO FREQUENCY NOISE

From the discussion so far, it should be clear that the carrier–envelope phase of a femtosecond oscillator is extremely sensitive towards any kind of environmental influence and also towards changes in the laser parameters, such as pulse duration or power fluctuations. In the following, we present measurements of the carrier–envelope-phase noise of a laser oscillator. From these measurements, one can judge the severity of the noise problem. It is also helpful to reach an understanding of the mechanisms behind the carrier–envelope-phase noise before attempting to stabilize the CEO phase. We set up the heterodyne detection scheme as previously described in detail. In most of the experiments, we use a Ti:sapphire oscillator similar to the setup described in [6]. One variant of the laser uses a sequence of two fused silica prisms in combination with chirped mirrors for dispersion compensation. Alternatively, we use the same laser converted to a prismless scheme, in which only chirped mirrors are employed for dispersion compensation. Both lasers deliver pulses in the 10- to 20-fs duration regime with a few 100 mW of output power. For the calculation of amplitude-to-phase coupling effects, the peak intensity inside the 2.3-mm long Ti:sapphire gain crystal is the decisive parameter. This value was measured as 4.5×10^{11} W/cm^2 for the laser with prisms and 10^{12} W/cm^2 for the prismless laser. Except for the mirrors used in the laser, the pump geometry and the mechanical setup were left widely unchanged to allow for a comparison of the two lasers.

To further quantify the CEO phase noise, we electronically convert the CEO frequency into a voltage by employing a phase-locked loop. This voltage is then spectrally analyzed with a dynamic signal analyzer (HP3562A). Multiplying the measured voltage noise by the conversion factor of the frequency-to-voltage converter yields the single-sideband frequency noise density $\sigma_{f_{CEO}}(f)$ in units Hz/$\sqrt{\text{Hz}}$ vs. offset frequency f. Figure 5 shows measurements of the CEO noise of the unstabilized laser with intracavity prisms and the prismless laser with and without stabilization. All measurements are composed of several sweeps with different spectral resolutions and are combined in a logarithmic plot, covering the range from 1 Hz to 100 kHz. The noise spectra typically show some discrete components at line frequency harmonics and a broad background reaching up to several kHz in the offset frequency. The laser with intracavity prisms shows by far the worst noise behavior, with a pronounced maximum centered at about 500 Hz. The prismless laser shows a more than ten-times improved passive stability. A further reduction of the noise can be achieved with active stabilization, which is shown for comparison and will be discussed below. For further interpretation of the results, it

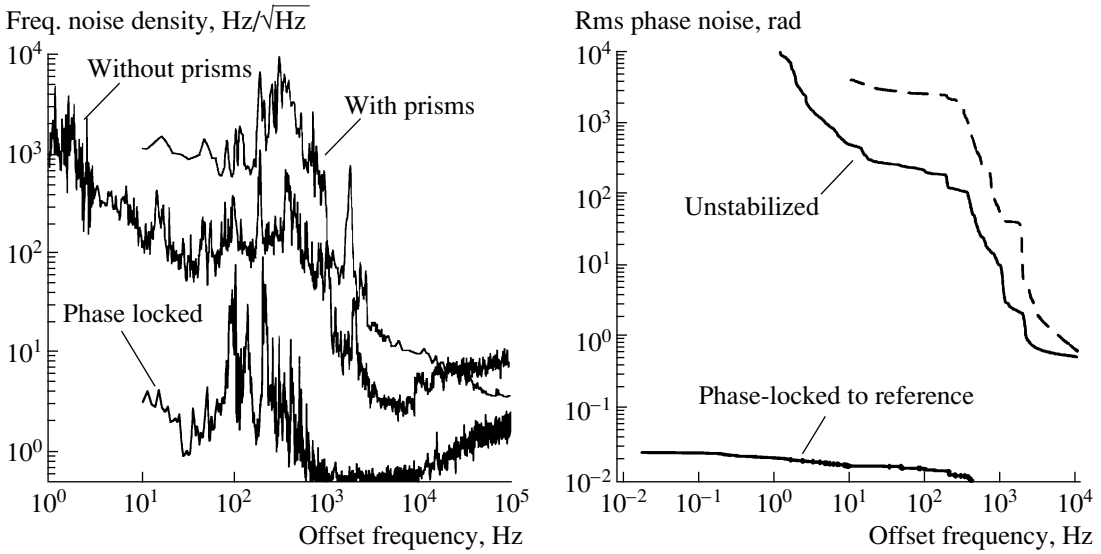

Fig. 5. Left: Carrier–envelope frequency noise density $\sigma_{f_{CEO}}$ as a function of offset frequency f. Right: rms phase noise $\delta_{\varphi_{CEO}}$ as a function of lower integration bound f_{low}. Both plots show the same three cases: a laser with intracavity prisms (top trace), a free-running prismless laser (middle trace), and a stabilized laser (bottom trace). The top two traces of the right graph were directly derived from the frequency noise measurements on the left side employing the f/U converter shown in Fig. 2. The bottom trace in the right graph was separately measured using homodyne detection with an rf lock-in amplifier.

is useful to convert the measured data into phase noise densities and to calculate rms values using

$$\delta_{\varphi_{CEO}} = \sqrt{2\int_{f_{low}}^{f_{rep}} \left(\frac{2\pi\sigma_{f_{CEO}}(f)}{f}\right)^2 df}. \qquad (12)$$

Effectively, the integration can only be carried from a variable lower bound f_{low} to the highest available offset frequency displayed in Fig. 5. However, as the noise rolls off very rapidly at high frequencies, the 100-kHz bandwidth of our analyzer does not preclude significant contributions to the rms phase jitter. In the case of active stabilization of the CEO frequency, a direct measurement of the phase noise density with an rf lock-in is generally far superior to the frequency-to-voltage conversion scheme described before. As a phase reference is available, a homodyne measurement provides much more reliable information at low offset frequencies. These homodyne noise measurements can be easily extended into the mHz range. We directly measured the phase noise jitter $\delta_{\varphi_{CEO}}$ with a Stanford SR844 rf lock-in (phase sample frequency 20 kHz). This is also shown in Fig. 5, together with the data calculated from the $\delta_{f_{CEO}}$ measurements for the free-running oscillator. From the comparison of the traces in this graph, one can see that, for integration times ($1/f_{low}$) well below a millisecond, the phase noise is always below 2π. Depending on the passive stability of the setup, the cumulated phase noise reaches 2π in the vicinity of f_{low} = 1 kHz. For a stable and effective phase lock, a roughly ten-times greater servo bandwidth is needed, i.e., f_{servo} > 10 kHz. The unstabilized curves exhibit a divergence towards zero frequency roughly following a $1/f$ dependence. In contrast, our measurements indicate that the CEO phase of the stabilized oscillator is always kept within an rms range of 20 mrad relative to the reference oscillator, regardless of integration time.

While a residual jitter of $\delta_{\varphi_{CEO}}$ = 0.02 rad is clearly the lowest value reported in the literature for extended observation times, one has to be well aware of the limitations of the measurement scheme employed. First, it has to be noted that, in the above measurements, the noise diagnostics and the stabilization circuitry were completely separated to allow for an independent check of the quality of the stabilization. However, the optical part of the measurement setup was not duplicated in these experiments. In particular, air turbulence in the Michelson interferometer may cause spurious drift components in the measured signal. We expect this not to be a severe effect, and it can be easily avoided by switching to a common path interferometer as used in single-shot CEO measurements. Another spurious contribution may stem from amplitude-to-phase coupling effects inside the microstructure fiber. From the CEO frequency noise-density measurements, one can estimate how much phase noise the very same element with identical amplitude-to-phase coupling causes if placed outside the laser cavity

$$\sigma_{\varphi_{CEO}}^{(\text{extracavity})} = \frac{2\pi}{f_{rep}}\sigma_{f_{CEO}}^{(\text{intracavity})}. \qquad (13)$$

This means that a sweep of the CEO frequency of an oscillator of one free spectral range corresponds to a

single-pass CEO phase change of 2π. Integrating over the frequency noise densities in Fig. 5, we can determine an estimate for the rms frequency jitter (20 Hz–100 kHz). We determine $\delta_{f_{CEO}} \approx 10$ kHz for the prismless laser and $\delta_{f_{CEO}} \approx 100$ kHz for the laser with prisms. Employing Eq. (13), this translates into extracavity contributions to the phase noise of $\delta_{\varphi_{CEO}} \approx 0.6$ and 6 mrad, respectively. This value would result if intracavity and extracavity amplitude-to-phase coupling have equal values. In other words, the extracavity coupling effects have to be at least 1000 times stronger than the intracavity effects to cause a loss of phase coherence between the input and output of the fiber in a 20-Hz bandwidth. This consideration is augmented by a recent measurement of fiber phase noise contributions, which were determined as $\delta_{\varphi_{CEO}} \approx 0.5$ rad in a 30-mHz bandwidth [16]. From both these observations, we conclude that the relative CEO phase drift between the fiber input and output is expected to be negligible within a 1-Hz bandwidth. One has to be aware, however, that the CEO phase of the continuum and of the laser itself may slowly drift apart on longer time scales, despite the stabilization. Similarly, interferometer noise may give rise to a slow drift on the time scale of minutes or above, but this can be greatly reduced in a common-path interferometer. These slow phase drift mechanisms should require some care in precision frequency metrology applications and have to be avoided. Further experiments are required to provide more precise information on the relative strength of the drift effects.

6. THE PHYSICAL ORIGIN OF CARRIER–ENVELOPE FLUCTUATIONS

In the previous sections, we analyzed carrier–envelope phase noise in great detail. From the observations reported so far, three main conclusions have to be drawn:

1. Lasers with intracavity prism sequences exhibit approximately ten-times higher noise levels than prismless oscillators.

2. There is evidence for nonlinear optical effects converting amplitude fluctuations of the laser into CEO phase fluctuations.

3. There are indications of fast and slow amplitude-to-phase coupling mechanisms. The fast mechanisms are most likely to be explained by self-refraction. Slower contributions may stem from thermally induced refractive changes.

In this paper, we want to focus on the self-refraction contribution to the phase noise. A detailed analysis of additional contributions caused by beam pointing fluctuations in intracavity prism sequences was reported in [20]. A closer comparison of thermal contributions to theory would require detailed modeling of the temperature profile in the gain medium. At low noise frequencies, the influence of atmospheric turbulence and pressure variations may give rise to phase noise contributions that are uncorrelated with power changes. The situation at higher noise frequencies, in contrast, is much cleaner and appears to be ruled by a single mechanism. This is confirmed by the observed reduction of laser power noise at frequencies above 2 kHz when activating the phase lock. At lower frequencies, such a reduction is not observed. These observations have also been reported by other groups [19]. It is well known that the refractive index of a dielectric material changes at high laser intensities [22]. Typically, the description of self-refraction is reduced to self-phase modulation along the axis of propagation, i.e., to a pure effect on the phase velocity v_φ of a medium. In certain cases, such as extremely short pulses, a nonlinear deformation of the pulse's envelope also needs to be considered. This is usually referred to as self-steepening and also effects the group velocity v_g of the dielectric medium. In the following, we want to find an estimate of how much the CEO phase of a pulse is affected by a change in laser intensity. For this purpose, we use the formalism developed in [23] for direct estimation of the linear dispersion of the Kerr effect in the frequency domain. This paper gives an analytic approach to calculating the frequency dependence of nonlinear refraction. At photon energies below half the band gap, the main contribution to nonlinear refraction stems from the Kramers–Kronig term induced by two-photon-absorption. Closer to the band gap, additional components have to be considered, such as Raman- and Stark-effect terms. Based on the complete model presented in [23], we calculated the nonlinear effect on the average group-phase offset of sapphire at a wavelength of 800 nm as $\omega dn^2/d\omega = 8 \times 10^{-21}$ m^2/W. This formalism also estimates self-refraction as $n_2 = 3 \times 10^{-20}$ m^2/W, which agrees very well with experimental data [24]. The computed group-phase offset leads to a theoretical value of $df_{CEO}/dI = 4 \times 10^{-9}$ Hz per W/m^2 for our laser. This agrees well with the measured value $df_{CEO}/dI \approx 10^{-8}$ Hz m^2/W in Fig. 3.

7. CONCLUSIONS

We have investigated fluctuations of the CEO phase in oscillators and explained some of the major driving forces behind this type of phase noise. On short time scales, nonlinear refraction is the main effect converting amplitude fluctuations into phase variations in prismless lasers. Additional effects caused by beam pointing fluctuation may be present in laser with intracavity prism sequences. As these effects can be much stronger than pure self-refractive mechanisms, prismless femtosecond oscillators should be used whenever the CEO stability is a concern. Based on our analysis, we achieved a phase lock of the CEO frequency to an external rf reference oscillator. The residual phase jitter between the laser and reference was found to be less than 20 mrad for integration times up to a minute. This

small jitter corresponds to a timing jitter between the carrier and envelope of approximately 10 attoseconds. The demonstrated control of the CEO phase with attosecond residual timing jitters is an important prerequisite for experiments in extreme nonlinear optics and precision frequency metrology.

The authors would like to thank R.S. Windeler, Lucent Technologies, for providing us with the microstructure fiber. We gratefully acknowledge the help of H.R. Telle, J. Stenger, and B. Lipphardt from the PTB Braunschweig precision frequency metrology group. This research was financially supported by ETH Zürich, grant no. 03159/41.

REFERENCES

1. Steinmeyer, G., Sutter, D.H., Gallmann, L., Matuschek, N., and Keller, U., 1999, *Science*, **2860**, 1507.
2. Nisoli, M., De Silvestri, S., Svelto, O., Szipöcs, R., Ferencz, K., Spielmann, C., Sartania, S., and Krausz, F., 1997, *Opt. Lett.*, **22**, 522.
3. Baltuška, A., Pshenichnikov, M.S., and Wiersma, D.A., 1998, *Opt. Lett.*, **23**, 1474.
4. Baltuška, A., Fuji, T., and Kobayashi, T., 2002, *Opt. Lett.*, **27**, 306.
5. Morgner, U., Ell, R., Metzler, G., Schibli, T.R., Kärtner, F.X., Fujimoto, J.G., Haus, H.A., and Ippen, E.P., 2001, *Phys. Rev. Lett.*, **86**, 5462.
6. Sutter, D.H., Steinmeyer, G., Gallmann, L., Matuschek, N., Morier-Genoud, F., Keller, U., Scheuer, V., Angelow, G., and Tschudi, T., 1999, *Opt. Lett.*, **24**, 631.
7. Paulus, G.G., Grasbon, F., Walther, H., Villoresi, P., Nisoli, M., Stagira, S., Priori, E., and De Silvestri, S., 2001, *Nature*, **414**, 182.
8. Brabec, T. and Krausz, F., 2000, *Rev. Mod. Phys.*, **72**, 545.
9. Telle, H.R., Steinmeyer, G., Dunlop, A.E., Stenger, J., Sutter, D.H., and Keller, U., 1999, *Appl. Phys. B*, **69**, 327.
10. Zhang, X.C., Hu, B.B., Darrow, J.T., and Auston, D.H., 1990, *Appl. Phys. Lett.*, **56**, 1011.
11. Baltuška, A., Fuji, T., and Kobayashi, T., 2002, *Phys. Rev. Lett.*, **88**, 133901.
12. Mehendale, M., Mitchell, S.A., Likforman, J.P., Villeneuve, D.M., and Corkum, P.B., 2000, *Opt. Lett.*, **25**, 1672.
13. Kakehata, M., Takada, H., Kobayashi, Y., Torizuka, K., Fujihira, Y., Homma, T., and Takahashi, H., 2001, *Opt. Lett.*, **26**, 1436.
14. Kakehata, M., Fujihira, Y., Takada, H., Kobayashi, Y., Torizuka, K., Homma, T., and Takahashi, H., 2002, *Appl. Phys. B*, **74**, S43.
15. Ranka, J.K., Windeler, R.S., and Stentz, A.J., 2000, *Opt. Lett.*, **25**, 25.
16. Fortier, T.M., Ye, J., Cundiff, S.T., and Windeler, R.S., 2002, *Opt. Lett.*, **27**, 445.
17. Helbing, F.W., Steinmeyer, G., Keller, U., Windeler, R.S., Stenger, J., and Telle, H.R., 2002, *Opt. Lett.*, **27**, 194.
18. Reichert, J., Holzwarth, R., Udem, T., and Hänsch, T.W., 1999, *Opt. Commun.*, **172**, 59.
19. Xu, L., Spielmann, C., Poppe, A., Brabec, T., Krausz, F., and Hänsch, T.W., 1996, *Opt. Lett.*, **21**, 2008.
20. Helbing, F.W., Steinmeyer, G., Stenger, J., Telle, H.R., and Keller, U., 2002, *Appl. Phys. B*, **74**, S35.
21. Poppe, A., Holzwarth, R., Apolonski, A., Tempea, G., Spielmann, C., Hänsch, T.W., and Krausz, F., 2000, *Appl. Phys. B*, **72**, 373.
22. Agrawal, G.P., 2001, *Nonlinear Fiber Optics*, 3rd ed. (San Diego: Academic).
23. Sheik-Bahae, M., Hutchings, D.C., Hagan, D.J., and Van Stryland, E.W., 1991, *IEEE J. Quantum Electron.*, **27**, 1296.
24. DeSalvo, R., Said, A.A., Hagan, D.J., Van Stryland, E.W., and Sheik-Bahae, M., 1996, *IEEE J. Quantum Electron.*, **32**, 1324.